Performance Improvement of Iterative Demodulation and Decoding for Spatially Coupling Data Transmission by Joint Sparse Graph

Zhengxuan Liu[1,2] , Guixia Kang[1,2] , Zhongwei Si[1] and Ningbo Zhang[1,2]
[1] Beijing University of Posts and Telecommunications
[2] Science and Technology on Information Transmission and Dissemination in Communication Networks Lab, Beijing, PR China
[E-mail: liuzhengxuan@bupt.edu.cn, gxkang@bupt.edu.cn]
*Corresponding author: Guixia Kang

Received May 29, 2016; revised September 22, 2016; accepted November 17, 2016; published December 31, 2016

Abstract

Both low-density parity-check (LDPC) codes and the multiple access technique of spatially coupling data transmission (SCDT) can be expressed in bipartite graphs. To improve the performance of iterative demodulation and decoding for SCDT, a novel joint sparse graph (JSG) with SCDT and LDPC codes is constructed. Based on the JSG, an approach for iterative joint demodulation and decoding by belief propagation (BP) is presented as an exploration of the flooding schedule, and based on BP, density evolution equations are derived to analyze the performance of the iterative receiver. To accelerate the convergence speed and reduce the complexity of joint demodulation and decoding, a novel serial schedule is proposed. Numerical results show that the joint demodulation and decoding for SCDT based on JSG can significantly improve the system's performance, while roughly half of the iterations can be saved by using the proposed serial schedule.

Keywords: Spatial coupling, joint sparse graph, belief propagation, density evolution, serial schedule

A preliminary version of this paper was presented at IEEE PIMRC 2016 on Sept. 4–8 in Valencia, Spain. The present version includes density evolution analysis for different system schemes and supporting implementation results based on density evolution. This work was supported by National Science and Technology Major Project of China(No. 2013ZX03006001, 2016ZX03001012) and National Natural Science Foundation of China(61501056).

http://dx.doi.org/10.3837/tiis.2016.12.015 **ISSN : 1976-7277**

1. Introduction

With the rapid development of mobile Internet technology and the Internet of Things, wireless communication now urgently needs spectral efficiency and sum capacity significant improvement. As the IMT-2020 Promotion Group proposed in the 2014 white paper "5G Vision and Requirements" [1], the future mobile communication system (5G) will supply the need for greater capacity by at least 1,000 times and improve spectral efficiency compared to 4G by 5–15 times. Recently, non-orthogonal multiple access (NOMA) technology has attracted the attention of researchers around the world. NOMA schemes can be divided into two categories—power-domain multiplexing and code-domain multiplexing—and the corresponding schemes include power-domain NOMA, sparse code multiple access, multi-user shared access, pattern division multiple access, and multiple access with low-density spreading, among other things, as summarized in [3]. These NOMA technologies were surveyed in [2]–[3], which formulated that NOMA could significantly improve spectral efficiency and system capacity compared to orthogonal multiple access used in 4G.

Low-density parity-check (LDPC) convolutional codes or so-called spatially coupled LDPC (SC–LDPC) codes introduced by Felström and Zigangirov [4] are the convolutional counterparts of LDPC block codes (LDPC–BC). Kudekar et al. [5] have proven that the belief propagation (BP) decoding threshold of an SC–LDPC code over the binary erasure channel could achieve the maximum a posteriori decoding threshold of the corresponding LDPC–BC, which they termed *threshold saturation via spatial coupling* [5]. Moreover, they confirmed that threshold saturation existed in all binary-input memory-less output-symmetric channels in [6]. Recently, the spatially coupled technique was successfully applied to the CDMA multiple-access channel [7]–[11], compressed sensing [12]–[13], the Slepian–Wolf coding problem [14], models in statistical physics [15], and in solutions to many other problems in communications and computer science.

To improve spectrum efficiency, research [7]–[11] has shown that the spatially coupled technique applied to multiple access channels could improve spectrum efficiency, since the achievable transmission rate for spatially coupling data transmission (SCDT) approaches the capacity of the additive white Gaussian noise (AWGN) channel by iterative bit estimation and interference cancellation, as shown in [7]–[8]. In [10]–[11], the performance of the BP receiver was improved to match the performance of individual optimal detection via spatially coupled sparse spreading. However, the demodulation complexity of [7]–[8] significantly increases along with the number of access datastreams. In [7] and [9], demodulation and decoding were performed separately, whereas [10]–[11] considered only iterative demodulation using BP or the Gaussian approximation (GA) BP-based algorithm. By contrast, this paper seeks to perform iterative demodulation and decoding simultaneously at the receiver.

Both SCDT and LDPC codes can be represented by bipartite graphs, which motivated us to combine SCDT with LDPC codes in order to construct a joint sparse graph (JSG). The constructed JSG includes variable nodes, channel nodes, and check nodes corresponding to encoded bits, received symbols, and parity-check equations of the LDPC code (i.e., assuming LDPC coding), respectively. Based on the entire sparse graph, the demodulation or decoding can use not only the knowledge of channels, but also parity-check information. Therefore, the joint demodulation and decoding for spatially coupling data transmission based on JSG (referred to as JSG–SCDT) might outperform the separated demodulation and decoding for SCDT (referred as to SDD–SCDT), since the demodulation and decoding of SDD–SCDT uses only the messages of the channel or parity-check.

In our previous work [16], the approach for iterative joint demodulation and decoding by BP was presented based on the graphical model by exploring the flooding schedule. Furthermore, a new serial schedule algorithm was proposed to accelerate the convergence speed and reduce the complexity. In [16], we analyzed the convergence behavior of different schedule schemes by using extrinsic information transfer (EXIT) charts. However, the threshold for the JSG–SCDT system can hardly be obtained by using EXIT charts. In order to obtain its threshold and show the evolution of the noise and interference power at different instances, in this paper density evolution (DE) is applied in the large sparse system limit, and the corresponding coupled DE equations are derived. Ultimately, more numerical results are presented to evaluate the proposed system performance from the different perspectives based on the derived DE equations.

In a related effort, the JSG was constructed by combining the multiple accesses of low-density signature-orthogonal frequency division multiplexing (LDS–OFDM) and LDPC codes in [17], which proposed design guidelines for JSG through an EXIT chart. The chief difference between this paper and [17] is that the multiple access of spatial coupling is applied in this paper instead of LDS–OFDM. The numerical results show that JSG–SCDT can bring about a 1-dB performance improvement compared with the uncoupled structure applied in [17]. In addition, the performance of iterative joint demodulation and decoding for the JSG–SCDT is analyzed by DE instead of with an EXIT chart. The spectral efficiency of JSG–SCDT can be analyzed easily by using the DE equation derived. In [23], a serial schedule for the iterative multi-user detection was proposed to decrease the number of detection iterations. However, few iterations are reduced for JSG–SCDT when only the messages of channel nodes are updated sequentially. Therefore, we proposed a novel serial schedule in which both channel nodes and check nodes were updated sequentially at the same time in order to accelerate the convergence speed of joint demodulation and decoding in [16]. To the best of our knowledge, the novel serial schedule applied in JSG–SCDT has never been considered before [16].

Throughout this paper, let notation p denote the probability density function (PDF), $\mathrm{E}[x]$ and $V[x]$ denote the mean and variance of a random variable x, respectively, and the superscript T denote the transpose of a vector or matrix.

The rest of this paper is organized as follows. Section 2 outlines system model, after which Section 3 presents the iterative joint demodulation and decoding by using the flooding schedule. Section 4 offers a performance analysis of JSG–SCDT and SDD–SCDT by applying DE, and Section 5 presents the proposed serial schedule and its algorithm. The performance evaluation of JSG–SCDT is provided by numerical simulation in Section 6. Lastly, Section 7 concludes the paper.

2. System Model

We consider that the SCDT is modulated by a superposition of L independent datastreams, which may be initiated by single or multiple users. The L-modulated streams add up with time to offset length t so that the spatially coupled datastreams are constructed.

Fig. 1 shows the transmitter block diagram of the SCDT system model. First, the binary information streams are encoded by LDPC codes. For notation brevity and simplicity, binary phase shift keying (BPSK) is used as the modulated scheme, after which the modulated symbols are divided into L datastreams, each with M symbols spread out by a spatially coupled

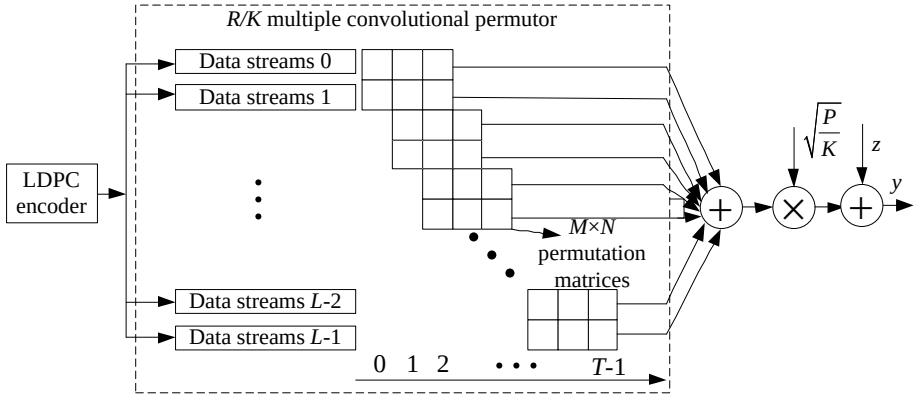

Fig. 1. Block diagram for spatially coupling data transmission, in which $R = 3$ and $K = 6$.

incidence matrix $\mathbf{H}$. $\mathbf{H}$ is constructed by an R/K multiple convolutional permutor (R/K MCP) [7], in which R and K correspond to the spreading length and maximum superposition datastreams, respectively. This method is similar to that used to construct SC–LDPC codes [18]. The R/K MCP contains R permutation matrices in each row and K permutation matrices in each column, except for a few columns at both ends. **Fig. 1** shows a 3/6 MCP in the dashed box, in which the spreading length is $R = 3$, and the maximum superposition datastreams are $K = 6$. The size of each permutation matrix is $M \times M$, represented by a blank square in the diagram. To prevent confusion and assure easy understanding in mathematical expressions, we use N to replace column M and define the ensemble of $\mathbf{H}$ as $C_H(R, K, M, N)$. Each row of R/K MCP multiplies a pseudo-random signature bit by bit before superposition in order to ensure that the modulated streams are uncorrelated. The maximal time length is denoted by T and the length of time offset by $t = N$, which corresponds to the column length of the permutation matrix. In this paper, the modulation load of the SCDT system is denoted by $\beta = K / R$, as defined in [7]. Ultimately, the output sequence is multiplied by the power normalizing amplitude $\sqrt{P / K}$ and transmitted over the AWGN channel. Without loss of generality, we assume $P = 1$.

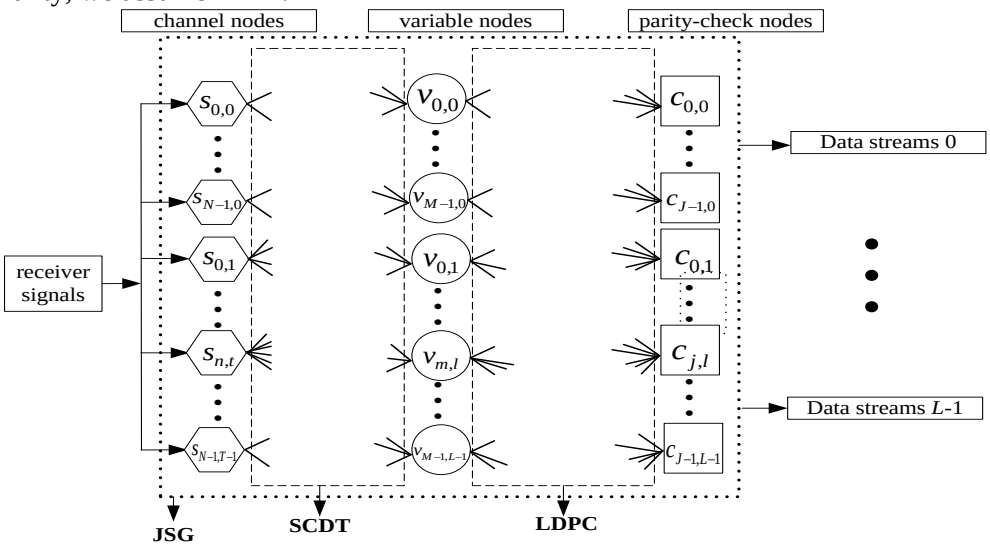

Fig. 2. The receiver of joint sparse graph for spatially coupling data transmission.

Since both the SCDT and LDPC codes can be represented by a factor graph, a JSG can be constructed for SCDT and LDPC codes. Thus, the joint iterative demodulation and decoding may be implemented on the JSG at the receiver. **Fig. 2** shows the receiver of JSG–SCDT, which is similar to that depicted in **Fig. 1** in [17]. In the figure, $v_{m,l}$, $s_{n,t}$ and $c_{j,l}$ denote the *m*-th variable node of the *l*-th stream, the *n*-th channel node during time *t*, and the *j*-th check node of the *l*-th stream, respectively, in which $m \in \mathcal{m} = \{0,\cdots,M-1\}$, $l \in \mathcal{l} = \{0,\cdots,L-1\}$, $n \in \mathcal{N} = \{0,\cdots,N-1\}$, $t \in \mathcal{T} = \{0,\cdots,T-1\}$, and $j \in \mathcal{J} = \{0,\cdots,J-1\}$. In the figure, the variable node, channel node, and check node corresponding to the data symbol and receiving the signal and parity-check equation are represented by a circle, hexagon, and square, respectively. At the receiver, the single graph labelled SCDT represents the spatially coupled incidence matrix H, whereas the other single graph labelled LDPC represents the parity-check matrices of the LDPC codes. Since the channel nodes and check nodes can be connected by variable nodes through edges, the receiver becomes a JSG labelled as such in **Fig. 2**. Note that fewer edges connect to the channel nodes at the both ends in the SCDT graph, which implies that less interference is induced by other datastreams on those channel nodes, which makes them obtain more reliable information. By extension, that reliable information can spread to the center of the JSG. Therefore, the channel nodes at the center of the JSG can also obtain reliable information. This dynamic is a remarkable advertage of SCDT over the conventional spreading sturcture applied in [17]. It is also noteworthy that the receiver of JSG–SCDT differs from that of the turbo-structure in that the demodulation and decdoing are performed by outer and inner iterations, respectively. For the receiver of JSG–SCDT, demodulation and decoding are implemented at the same time on the JSG in each iteration. Hence, the JSG–SCDT is based on a JSG that combines coupling data transmission and coding techniques.

Let $y_{n,t}$ denote the received signal at *n* point during time *t*. Accordingly, the received signal $\mathbf{y}_t = (y_{0,t},\cdots,y_{n,t},\cdots,y_{N-1,t})^T \in \mathbb{R}^N$ during time *t* can be formulated by

$$\mathbf{y}_t = \sum_{l\in\mathcal{l}} \sum_{m\in\mathcal{m}} \frac{1}{\sqrt{K}} \mathbf{s}_{t,m,l} b_{m,l} + \mathbf{z}_t, \tag{1}$$

in which the vector $\mathbf{z}_t \sim \mathcal{N}(\mathbf{0}_{N\times 1}, \sigma_z^2 \mathbf{I}_{N\times 1})$ denotes the AWGN vector with variance σ_z^2. The *N*-dimensional vector $\mathbf{s}_{t,m,l} = (s_{0,t,m,l},\cdots,s_{N-1,t,m,l})^T$ represents the spreading sequence of the *m*-th data symbol for the *l*-th stream during time *t*, while $b_{m,l} \in \{-1,+1\}$ denotes the *m*-th BPSK data symbol for the *l*-th stream. Let $\mathbf{Y} = (\mathbf{y}_0,\cdots,\mathbf{y}_{T-1})^T$, $\mathbf{b}_l = \left(b_{0,l},\cdots,b_{M-1,l}\right)^T$, $\mathbf{B} = \left(\mathbf{b}_0,\cdots,\mathbf{b}_{L-1}\right)^T$, $\mathbf{S}_{t,l} = (\mathbf{s}_{t,0,l},\cdots,\mathbf{s}_{t,M-1,l})$, and $\mathbf{Z} = (\mathbf{z}_0,\cdots,\mathbf{z}_{T-1})^T$. The system (1) can also be formulated as

$$\mathbf{Y} = \frac{1}{\sqrt{K}} \mathbf{H}\mathbf{B} + \mathbf{Z} \tag{2}$$

in which

$$\mathbf{H}=\begin{bmatrix} \mathbf{s}_{0,0} & \cdots & \mathbf{s}_{0,\beta-1} & & & & \\ \vdots & \ddots & & \ddots & & & \\ \mathbf{s}_{R-1,0} & \cdots & \mathbf{s}_{R-1,\beta-1} & & \ddots & & \\ & & & \ddots & & \ddots & \\ & & & & \mathbf{s}_{T-1,L-\beta} & \cdots & \mathbf{s}_{T-1,L-1} \end{bmatrix}$$

and the blank spaces of $\mathbf{H}$ correspond to zeros.

3. Iterative Joint Demodulation and Decoding

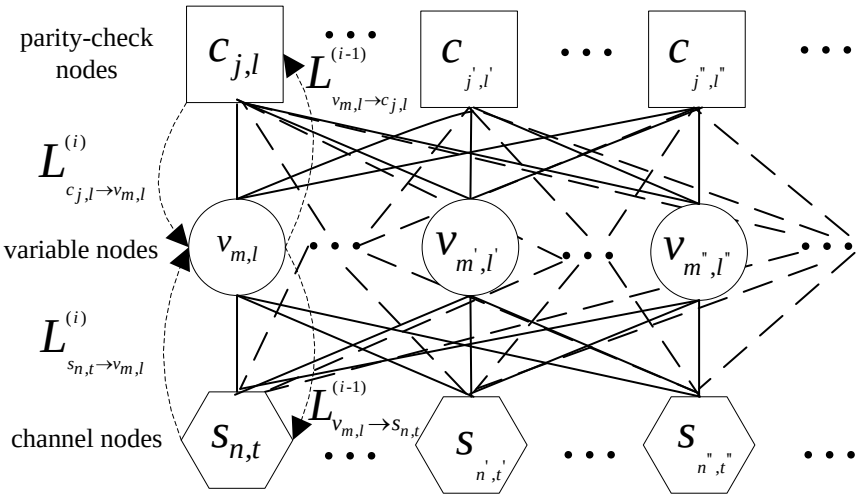

Fig. 3. Messages passing in the joint sparse graph for spatially coupling data transmission.

3.1 Messages Passing in the Joint Sparse Graph

The messages passing via different types of nodes on one JSG for the JSG–SCDT is depicted in **Fig. 3**. In our proposal, there is an edge connecting the variable node and channel node if the corresponding element is non-zero in spreading matrix **H**. Similarly, there is an edge connecting the variable node and check node if the former satisfies the parity-check equation. The dashed lines in **Fig. 3** represent the possible variable nodes connected to check or channel nodes. The number of edges connected to the channel node equals the number of superposition symbols at one point during time *t*, whereas the number of edges connected to the check node equals its degree in the parity-check matrix. Let $L^{(i)}_{\bullet\to\bullet}$ denote the log likelihood ratio (LLR) delivered from one node to the other in iteration *i*, meaning that $L^{(i)}_{s_{n,t}\to v_{m,l}}$ ($L^{(i)}_{c_{j,l}\to v_{m,l}}$) denotes the LLR delivered from channel node $s_{n,t}$ (check node $c_{j,l}$) to variable node $v_{m,l}$ in iteration *i*, and $L^{(i-1)}_{v_{m,l}\to s_{n,t}}$ ($L^{(i-1)}_{v_{m,l}\to c_{j,l}}$) denotes the LLR delivered from variable node $v_{m,l}$ to channel node $s_{n,t}$ (check node $c_{j,l}$) in iteration *i*-1. As the figure shows, the message of the variable node $L^{(i-1)}_{v_{m,l}\to s_{n,t}}$ ($L^{(i-1)}_{v_{m,l}\to c_{j,l}}$) sent to the channel node or check node includes the messages of the check and channel nodes in iteration *i*. By contrast, the message of the check and channel nodes are

updated in iteration *i* by using the updated message from the variable node in the last iteration. Therefore, the demodulation or decoding of JSG–SCDT can use not only the knowledge of channels, but also parity-check information on one JSG, which indicates that the method can improve system performance and accelerate convergence speed.

In graphical models, the BP algorithm is feasible for calculating the marginal distribution for each node and can compute the exact marginal posterior probabilities if there are no cycles in the graph [19]. However, it usually contains cycles in single graphs such as LDPC codes and SCDT. For LDPC coding, it is necessary to design the degree distribution carefully so that the short cycles are avoided in the graph. The design of the degree distribution to achieve more gains and avoid cycles is a promising future direction, but it is beyond the scope of this paper. For the SCDT, if the $C_H\left(R,K,M,N\right)$-ensemble is constructed carefully, then it might have the crucial asymptotic cycle-free (ACF) property in the large-system limit, in which *R* and *K* tend toward infinity, whereas $\beta = K/R$ is kept constant after taking $L \to \infty$. Following the instructions of [20]–[21], we let the superposition datastreams *K* grow as slowly as $O\left(L^{1/(4t)}\right)$ with *L*, with the probability that $b_{m,l}$ is involved in a cycle of length shorter than *t* and approaches zero as $K = \beta R$ is kept constant after taking $L \to \infty$. Note that the system is sparse even though $K \to \infty$, since the large-system limit is taken first. In that way, the constructed $C_H\left(R,K,M,N\right)$-ensemble satisfies the ACF property. In this paper, the large-system limit with $K = \beta R$, $L \to \infty$ is defined as the large sparse system limit. Since the $C_H\left(R,K,M,N\right)$-ensemble satisfies the ACF property, there are no cycles with finite length in the large sparse system limit [11]. Therefore, the BP receiver is guaranteed to converge in the infinite iteration limit after taking the large sparse system limit in the iterative joint demodulation and decoding. Note that the two limits do not commute with each other.

3.2 Messages Updated in the Flooding Schedule for JSG–SCDT

The mathematical expressions of messages updated for various nodes are given and described as follows. Let ∂, β, ψ and φ denote the set corresponding to various nodes and $\partial(\bullet)\backslash(*)$ denote the set of $\bullet$ nodes excluding the * node. For instance, $\partial(n,t)$ and $\partial(n,t)\backslash(m,l)$ denote the set of variable nodes connected to channel node $s_{n,t}$ and the set of variable nodes connected to channel node $s_{n,t}$, excluding $v_{m,l}$, respectively. In (4), $\mathbf{B}_{[n,t]}$ and $\mathbf{H}_{[n,t]}$ denote the vector stacking of symbols transmitted and their corresponding signature vector at *n* point during time *t*, respectively. The messages updated among various nodes via edges by applying flooding schedule for the JSG–SCDT are described as follows.

A. Initialization

Assuming no a priori probabilities available,

$$L^{(0)}_{v_{m,l}\to s_{n,t}} = 0, L^{(0)}_{v_{m,l}\to c_{j,l}} = 0, \forall m, \forall l, \forall n, \forall t, \forall j. \tag{3}$$

B. **Updating of Channel Nodes and Check Nodes**

The LLR of the channel nodes is updated by

$$L_{s_{n,t}\to v_{m,l}}^{(i)}=\ln\frac{\sum\limits_{\substack{\{b_{\tilde{m},\tilde{l}}\}\\ b_{m,l}=1}}\exp\left(\sum\limits_{(\tilde{m},\tilde{l})\in\partial(n,t)\backslash(m,l)}\frac{b_{\tilde{m},\tilde{l}}L_{v_{\tilde{m},\tilde{l}}\to s_{n,t}}^{(i-1)}}{2}-\frac{\left\|y_{n,t}-\frac{\mathbf{H}_{[n,t]}\mathbf{B}_{[n,t]}}{\sqrt{K}}\right\|^2}{2\sigma_z^2}\right)}{\sum\limits_{\substack{\{b_{\tilde{m},\tilde{l}}\}\\ b_{m,l}=-1}}\exp\left(\sum\limits_{(\tilde{m},\tilde{l})\in\partial(n,t)\backslash(m,l)}\frac{b_{\tilde{m},\tilde{l}}L_{v_{\tilde{m},\tilde{l}}\to s_{n,t}}^{(i-1)}}{2}-\frac{\left\|y_{n,t}-\frac{\mathbf{H}_{[n,t]}\mathbf{B}_{[n,t]}}{\sqrt{K}}\right\|^2}{2\sigma_z^2}\right)}. \tag{4}$$

The LLR of the check nodes is updated by

$$L_{c_{j,l}\to v_{m,l}}^{(i)}=\ln\frac{1+\prod\limits_{(\tilde{m},\tilde{l})\in\psi(j,l)\backslash(m,l)}\tanh\left(\frac{L_{v_{\tilde{m},\tilde{l}}\to c_{j,l}}^{(i-1)}}{2}\right)}{1-\prod\limits_{(\tilde{m},\tilde{l})\in\psi(j,l)\backslash(m,l)}\tanh\left(\frac{L_{v_{\tilde{m},\tilde{l}}\to c_{j,l}}^{(i-1)}}{2}\right)}. \tag{5}$$

C. **Updating of Variable Nodes**

Since the LLR of variable nodes not only receives channel nodes messages, but also includes check node information on one JSG, the LLR delivered to the channel node from the variable node is given by

$$L_{v_{m,l}\to s_{n,t}}^{(i)}=\sum_{(\tilde{n},\tilde{t})\in\beta(m,l)\backslash(n,t)}L_{s_{\tilde{n},\tilde{t}}\to v_{m,l}}^{(i)}+\sum_{(\tilde{j},\tilde{l})\in\varphi(m,l)}L_{c_{\tilde{j},\tilde{l}}\to v_{m,l}}^{(i)}. \tag{6}$$

The LLR delivered to the check node from the variable node is given by

$$L_{v_{m,l}\to c_{j,l}}^{(i)}=\sum_{(\tilde{n},\tilde{t})\in\beta(m,l)}L_{s_{\tilde{n},\tilde{t}}\to v_{m,l}}^{(i)}+\sum_{(\tilde{j},\tilde{l})\in\varphi(m,l)\backslash(j,l)}L_{c_{\tilde{j},\tilde{l}}\to v_{m,l}}^{(i)}. \tag{7}$$

D. **Estimation and Syndrome Computing**

The posteriori probability of the transmitted symbol $v_{m,l}$ is given by

$$L_{v_{m,l}}=\sum_{(\tilde{n},\tilde{t})\in\beta(m,l)}L_{s_{\tilde{n},\tilde{t}}\to v_{m,l}}^{(I)}+\sum_{(\tilde{j},\tilde{l})\in\varphi(m,l)}L_{c_{\tilde{j},\tilde{l}}\to v_{m,l}}^{(I)}, \tag{8}$$

in which I denotes the maximum number of iterations. A hard decision based on the LLR message can be made by $\hat{v}_{m,l}=\arg\max\limits_{v_{m,l}}L_{v_{m,l}}$.

The iterative joint demodulation and decoding process ends when the result of syndrome computing for each user equals 0, even if the maximum number of iteration has not been reached, which indicates that the number of iterations can be reduced.

4. Density Evolution

4.1 DE of Joint Demodulation and Decoding

The asymptotic PDF of LLRs delivered from the decoder can be analyzed with the GA of the LLRs [22], whereas the PDF of LLRs emitted from the demodulator can be analyzed not only with the exact BP algorithm, but also with the GA BP-based algorithm [11]. We follow [11] to present the DE of iterative demodulation for the JSG–SCDT. The equivalent channel between $b_{m,l}$ and the corresponding output in iteration i is given by

$$p\left(b_{m,l}^{(i)}\middle|b_{m,l}\right)=\overline{\int p^{(i)}\left(b_{m,l}=b_{m,l}^{(i)}\middle|\mathcal{Y},\mathbf{H}\right)p\left(\mathcal{Y}\middle|\mathbf{H},b_{m,l}\right)d\mathcal{Y}},\tag{9}$$

in which $\mathcal{Y}=\{\mathbf{y}_t : t\in\mathcal{T}\}$. The horizontal line represents the expectation with respect to **H**. We prove that the equivalent channel (9) for the BP receiver in iteration *i* converges to a scalar AWGN channel in the large sparse system limit. The scalar AWGN channel is given by

$$z_{m.l}^{(i)}=b_{m,l}+w_{m,l}^{(i)},\tag{10}$$

in which $w_{m,l}^{(i)}\sim\mathcal{N}(0,(sir_l^{(i)})^{-1})$, in which $sir_l^{(i)}$ will be defined. Theorem 1 and coupled equations are given as follows.

Theorem 1: Suppose that **H** is picked up from the $C_H\left(R,K,M,N\right)$-ensemble and that the equivalent channel (9) for the BP joint demodulation and decoding based on JSG in iteration *i* converges to the equivalent channel for the scalar AWGN channel (10) in the large sparse system limit. DE equations are given by the coupled equations:

$$sir_l^{(i)}=\tilde{sir}_l^{(i)}+\frac{d_v}{2}\rho_u^{(i)},\tag{11}$$

$$\sigma_t^2(i)=\sigma_z^2+\frac{1}{K}\sum_{k=0}^{K_t-1}\zeta(sir_{[k+(t-R+1)\beta]}^{(i-1)})\tag{12}$$

with $sir_l^{(0)}=0$ for all $l\in\mathcal{U}$ and $\left(t-R+1\right)\beta=0$ when $t<=1$. In (11) and (12)

$$\tilde{sir}_l^{(i)}=\frac{1}{K}\sum_{r=0}^{R-1}\frac{1}{\sigma_{(r+\lfloor l/\beta\rfloor)}^2(i)},\tag{13}$$

$$\rho_u^{(i)}=\Phi^{-1}\left(1-[1-\Phi(\rho_{u_0}^{(i-1)}+(d_v-1)\rho_u^{(i-1)})]^{d_c-1}\right),\tag{14}$$

$$\zeta\left(sir_l^{(i)}\right)=\mathrm{E}[(b_{m,l}-\mathrm{E}[b_{m,l}^{(i)}])^2].\tag{15}$$

In (11)–(15), $\tilde{sir}_l^{(i)}$, $\sigma_t^2(i)$, $\rho_u^{(i)}$, and $\rho_{u_0}^{(i)}$ denote the signal-to-interference ratio (SIR) of the *l*-th stream from the BP demodulation, the interference and noise variance during time *t*, the mean of the output LLR u of a check node, and the output LLR u_0 of the output bit associated with the variable node in iteration *i*, respectively. The number of superposition datastreams at one point during time *t* is denoted by K_t, $K_t\in[\beta,K]$ for all $t\in\mathcal{T}$. In (13), $\lfloor\bullet\rfloor$ denotes the bottom integer function. Following [22], we derive (14), in which $\Phi(x)$ is the function defined in [22] and $\rho_{u_0}^{(i)}=2\tilde{sir}_l^{(i)}b_{m,l}$. The degrees of the variable and check nodes are denoted by d_v and d_c, respectively. In (15), $\mathrm{E}[b_{m,l}^{(i)}]$ denotes the posterior mean estimator of $b_{m,l}$ in iteration *i* and is given by

$$\mathrm{E}[b_{m,l}^{(i)}]=\sum_{b_{m,l}=\pm1}b_{m,l}\,p(b_{m,l}\left|z_{m.l}^{(i)}\right.)=\tanh(sir_l^{(i)}z_{m.l}^{(i)}).\tag{16}$$

Proof: See the Appendix.

Theorem 1 implies that the problem of estimating each data symbol $b_{m,l}$ using BP in iterations *i* for the JSG–SCDT is asymptotically equivalent to estimating the same symbol through a scalar Gaussian channel with SIR equal to $sir_l^{(i)}$.

Remark 1: If an ensemble used has the ACF property in the large sparse system limit, then [11, Theorem 2] has proven that the equivalent channel for the BP demodulation with GA converges with the asymptotic equivalent channel for the exact BP demodulation. Since the

$C_H(R,K,M,N)$-ensemble has a similar property with the ensemble defined in [11] in the large sparse system limit, the exact BP demodulation is applied to prove Theorem 1.

4.2 DE of Separated Demodulation and Decoding

In the SDD–SCDT scheme, since coding makes no essential change in the analysis of iterative receivers, we focus on the iterative demodulation by the BP receiver. We prove that equivalent channel (9) also equals channel (10) in the large sparse system limit. However, the noise variance of channel (10) equals $\left(\widehat{sir}_l^{(i)}\right)^{-1}$, meaning that $\widehat{sir}_l^{(i)}$ and Theorem 2 are presented as follows.

Theorem 2: Suppose that **H** is picked up from the $C_H(R,K,M,N)$-ensemble. The equivalent channel (9) for the BP demodulation of the SDD–SCDT in iteration i converges to the equivalent channel for the scalar AWGN channel (10) with the noise variance $\left(\widehat{sir}_l^{(i)}\right)^{-1}$ in the large sparse system limit. DE equations are written as the coupled equations

$$\widehat{sir}_l^{(i)} = \frac{1}{K}\sum_{r=0}^{R-1}\frac{1}{\widehat{\sigma}^2_{(r+\lfloor l/\beta \rfloor)}(i)}, \tag{17}$$

$$\widehat{\sigma}_t^2(i) = \sigma_z^2 + \frac{1}{K}\sum_{k=0}^{K_t-1}\zeta\left(\widehat{sir}^{(i-1)}_{[k+(t-R+1)\beta]}\right). \tag{18}$$

Proof: The proof of Theorem 2 is included in the proof of Theorem 1.

As a comparison of expressions (11)–(17) shows, the SIR of JSG–SCDT includes not only the SIR of BP demodulation, but also the SIR of BP decoding. That circumstance indicates that the performance and convergence speed of the JSG–SCDT might outperform the SDD–SCDT. To futher accelerate the convergence speed of JSG–SCDT, in the next section we propose a novel serial schedule to update all channel and check node messages sequentially.

5. Serial Schedule

In subsection 3.2, the flooding schedule is applied to update all channel and check node messages in parallel. For the flooding schedule, the messages of all channel and check nodes are updated at the same time, after which the messages of all variable nodes are updated simultaneously. All updated messages have to be stored in the current iteration so that they are used in the next iteration, which implies that the new updated messages cannot be used at once during the message-passing process. Therefore, the convergence speed is slow, and the detection performance is limited. In addition, all updated messages have to be stored in the current iteration. Thus, more large memory registers are needed to store the hardware implementation in practice, which increases the hardware cost.

The message-passing schedule is a key factor that influences convergence speed and system performance [23]. The authors in [23] proposed a schedule algorithm by which new updated messages of channel nodes can be joined into the BP process immediately. However, the convergence speed accelerated is rather limited by using the algorithm proposed in [23] for JSG–SCDT. The messages of check nodes can also be updated by using a similar schedule due to BP decoding. Thus, we proposed a novel serial schedule by which both channel and check nodes update their messages sequentially on one JSG.

In the serial schedule, $L_{v_{m,l}\to s_{n,t}}^{(i-1)}$ and $L_{v_{m,l}\to c_{j,l}}^{(i-1)}$ are computed by $L_{v_{m,l}}^{(i)}$, $L_{s_{n,t}\to v_{m,l}}^{(i-1)}$ and $L_{v_{m,l}}^{(i)}$, $L_{c_{j,l}\to v_{m,l}}^{(i-1)}$, respectively, on the fly, in which $L_{v_{m,l}}^{(i)}$ denotes the LLR of the transmitted symbol $v_{m,l}$ in iteration ***i***. For instance, the message of the channel node is updated in the serial schedule as

$$L_{v_{m,l}\to s_{n,t}}^{(i-1)} = L_{v_{m,l}}^{(i)} - L_{s_{n,t}\to v_{m,l}}^{(i-1)}. \tag{19}$$

Substituting (19) into (4), the new updated message $L_{s_{n,t}\to v_{m,l}}^{(i)}$ of the channel node is obtained. The message of the transmitted symbol is updated by applying the new message of the channel node according to (20).

$$L_{v_{m,l}}^{(i_{new})} = L_{v_{m,l}}^{(i_{old})} - L_{s_{n,t}\to v_{m,l}}^{(i-1)} + L_{s_{n,t}\to v_{m,l}}^{(i)} \tag{20}$$

The message of the check node is updated similarly. The detailed procedures of the novel serial schedule are presented in Algorithm 1.

Algorithm 1: The serial schedule

1: **Initialization:**
2: $L_{v_{m,l}}^{(1)} = 0, L_{s_{n,t}\to v_{m,l}}^{(0)} = 0, L_{c_{j,l}\to v_{m,l}}^{(0)} = 0, \forall m, \forall l, \forall n, \forall t, \forall j.$
3: **For** i=1, $i \le I$,i++ **do**
4: // Updating of channel nodes in the serial schedule
5: **For all** $v_{m,l}$, $s_{n,t}$ **do**
6: $L_{v_{m,l}\to s_{n,t}}^{(i-1)} = L_{v_{m,l}}^{(i)} - L_{s_{n,t}\to v_{m,l}}^{(i-1)}$;
7: Updating $L_{s_{n,t}\to v_{m,l}}^{(i)}$ by using (4);
8: $L_{v_{m,l}}^{(i)} = L_{v_{m,l}}^{(i)} - L_{s_{n,t}\to v_{m,l}}^{(i-1)} + L_{s_{n,t}\to v_{m,l}}^{(i)}$;
9: **End for**
10: // Updating of check nodes in the serial schedule
11: **For all** $v_{m,l}$, $c_{j,l}$ **do**
12: $L_{v_{m,l}\to c_{j,l}}^{(i-1)} = L_{v_{m,l}}^{(i)} - L_{c_{j,l}\to v_{m,l}}^{(i-1)}$;
13: Updating $L_{c_{j,l}\to v_{m,l}}^{(i)}$ by using (5)
14: $L_{v_{m,l}}^{(i)} = L_{v_{m,l}}^{(i)} - L_{c_{j,l}\to v_{m,l}}^{(i-1)} + L_{c_{j,l}\to v_{m,l}}^{(i)}$;
15: **End for**
16: **End for**
17: **Return** $\hat{v}_{m,l} = \arg\max_{v_{m,l}} L_{v_{m,l}}^{(\mathrm{I})}$.

Compared with the flooding schedule, more new updated messages are used in the serial schedule. For instance, lines 5–15 in Algorithm 1 show that the new updated information of the channel and check nodes can join message-passing immediately, which makes both other channel and check nodes use fresh messages in the current iteration. Thus, the proposed serial schedule can be more efficient in terms of convergence speed and system performance. Due to the faster convergence speed that reduces the number of iterations needed, receiver complexity is less than that of the flooding schedule. Moreover, according to Algorithm 1, more large memory registers are not needed to store $L_{v_{m,l}\to s_{n,t}}^{(i)}$ and $L_{v_{m,l}\to c_{j,l}}^{(i)}$, which can reduce hardware

costs. Note that the flooding schedule has inherent advantages for hardware implementation; for instance, the parallelization of the algorithm for high speeds can be implemented. For the serial schedule, such a dynamic causes longer processing delays than in the flooding schedule. To solve that problem, so-called window decoding, which is used to decode spatially coupled LDPC codes, is an efficient, low-complexity, and low-delay technique that requires less memory. Since spatially coupling data transmission also has the spatially coupled feature and the messages are updated in a pipelined manner for the serial schedule, joint demodulation and decoding may be implemented by using window decoding to reduce decoding latency, which is hereby left for future investigations.

6. Performance Evaluation

For simplicity's sake, a half-rate (3, 6)-regular LDPC code and $C_H\left(3,6,100,100\right)$-ensemble is adopted in all numerical results except special statements. The flooding schedule is applied to analyze the performance of the JSG–SCDT except in subsection 6.3 and **Fig. 9**.

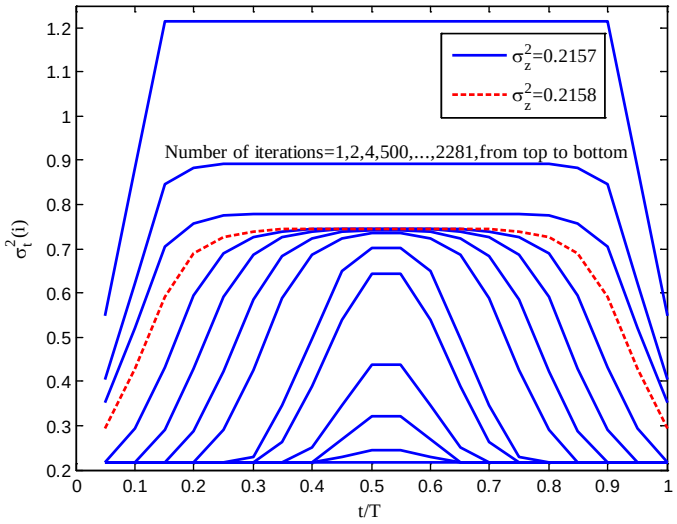

Fig. 4. Interference and noise variance $\sigma_t^2(i)$ versus t/T for the joint sparse graph for spatially coupling data transmission, $L=36$; solid lines denote the $\sigma_t^2(i)$ for $\sigma_z^2=0.2157$, whereas the red dashed line shows $\sigma_t^2(i)$ for $\sigma_z^2=0.2157$ and $i=10^5$.

6.1 Density Evolution Analysis

Fig. 4 shows the evolution of $\sigma_t^2(i)$ based on Theorem 1. Clearly, there is less interference at boundaries *t*/*T*=0 and *t*/*T*=1 than at the other positions in the first few iterations. However, the interference of other positions decreases dramatically as i increases; the interference at the center *t*/*T*=0.5 is approximately equal to σ_z^2 after a certain number of iterations, which implies that the inter-stream interference has been eliminated completely. When $\sigma_z^2\geq 0.2158$, by contrast, $\sigma_t^2(i)$ tends toward a value distant from σ_z^2 at the center *t*/*T*=0.5 after enough

iterations (i.e., $i=10^5$). This dynamic implies that the system is interference limited for $\sigma_z^2 \geq 0.2158$, and therefore, the decoding threshold is between 0.2157 and 0.2158.

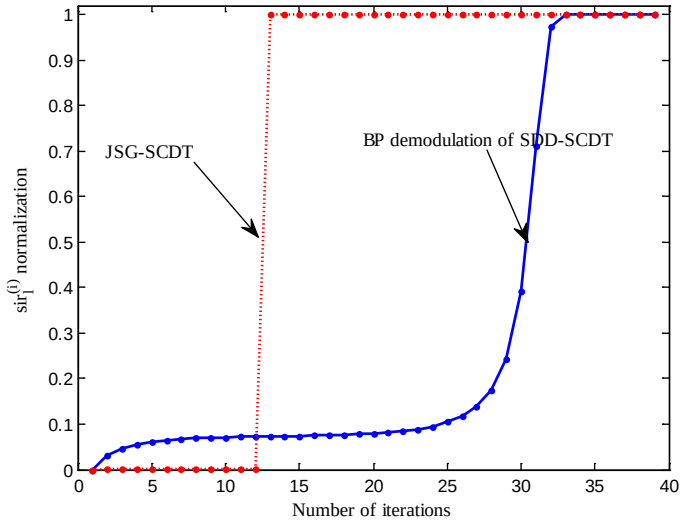

Fig. 5. The normalization $sir_l^{(i)}$ versus number of iterations at the center $1/L=0.5$, $L=36$, $\sigma_z^2=0.0312$ .The solid and dashed-dotted lines denote the normalization of the signal-to-interference ratio (SIR) of the joint sparse graph for spatially coupling data transmission (SCDT) and the demodulation of the separated demodulation and decoding for SCDT.

Fig. 5 depicts the convergence behavior of SIRs for the JSG–SCDT and BP demodulation for the SDD–SCDT, in which SIRs are calculated based on Theorems 1 and 2, respectively. The SIRs of the JSG–SCDT converge in iteration 13, whereas the BP demodulation of the SDD–SCDT needs 33 iterations, because the messages of channels and decoding are included in the BP receiver of the JSG–SCDT, whereas the BP demodulation of the SDD–SCDT uses only the information of channels. As such, it needs fewer iterations to converge for JSG–SCDT. Note that convergence means that the interference among datastreams has been canceled completely. In fact, the iteration has been terminated before 13 iterations for JSG–SCDT due to syndrome computing in practical systems, as verified in subsection 6.3.

Table 1. Decoding thresholds for the joint sparse graph (JSG) for spatially coupling data transmission (SCDT), separated demodulation and decoding for SCDT, and the JSG for conventional structure (CONV), in which $R=3$ and $K=6$.

Schemes	**SDD–SCDT**	**JSG–CONV**	**JSG–SCDT**			
L	36	36	18	36	72	108
σ_z^2	0.0649	0.1323	0.2158	0.2157	0.2157	0.2157
β_a	1.8	2	1.636	1.8	1.895	1.929

Table 1 lists the decoding thresholds of finite-sized systems for the JSG–SCDT, SDD–SCDT, and JSG–CONV, the last of which is a conventional structure (i.e., without spatial coupling) based on the JSG. The thresholds of the JSG–SCDT and JSG–CONV can be estimated by Theorem 1 numerically. Let β_a denote the actual modulation load. Due to the

influence of the rate of loss on both ends for SCDT, β_a is <2 for the SCDT. Therefore, the decoding threshold of the JSG–SCDT for L = 18 is larger than for the others. When the datastreams L are set to 36, 72, and 108 for the JSG–SCDT, the decoding threshold for all are identical, meaning that L = 36 has nearly eliminated the influence of the rate of loss. It is well known that the LLR message u_0 from the channel is a Gaussian distribution with mean $2/\sigma_{GA}^2$, in which σ_{GA}^2 calculated by GA [22] is the decoding threshold of LDPC codes. Thus, the decoding threshold of SDD–SCDT can be obtained by $\mathrm{E}\left(\widehat{sir}_l^{(I)}\right)=1/\sigma_{GA}^2$ based on Theorem 2. Clearly, both spatial coupling and joint demodulation and decoding based on the JSG can significantly improve the decoding threshold compared with a conventional structure and SDD, respectively.

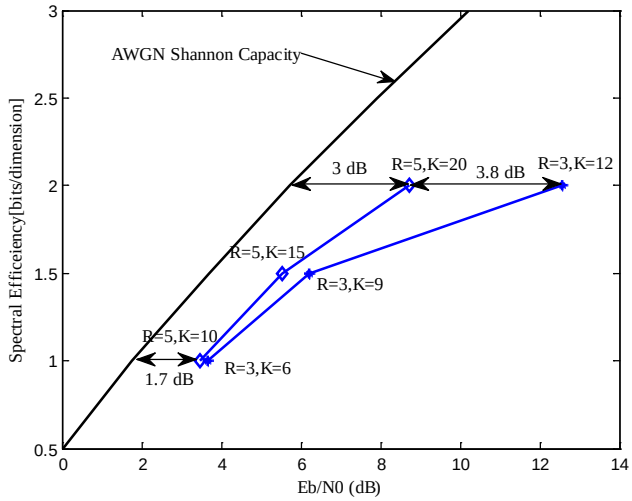

Fig. 6. Spectral efficiency versus signal-to-noise ratio (in dB) for different modulation loads.

6.2 Spectral Efficiency Analysis

Spectral efficiency for the JSG–SCDT versus signal-to-noise ratio (SNR) for higher modulation loads is plotted in **Fig. 6**. Datastreams L are set to be large enough to reduce the influence of the rate of loss. The curve with stars corresponds to $\beta=2$, 3, and 4, in which $R=3$ and $K=6$, 9, and 12. The curve with diamonds plots spectral efficiency achieved by $R=5$ and $K=10$, 15, and 20, and the AWGN's Shannon capacity is represented by the solid black curve. Only 1.7 dB of distance separates the Shannon capacity when β = 2, and the gap between the curve with $R=3$ or $R=5$ and Shannon capacity becomes larger as β increases, which indicates that the lower the modulation load, the closer the JSG operates toward Shannon capacity. This dynamic is due to interference among datastreams, which increases as the superposition datastreams increase for higher modulation loads. However, when the modulation load is high, the gap can be reduced by increasing the repeat number R. For instance, compared to ($R=3$, $K=12$), ($R=5$, $K=20$) can induce a 3.8-dB improvement in performance when β =4, and there is roughly only 3 dB of distance from the Shannon capacity. That circumstance implies that increasing R can effectively combat interference among datasteams. By contrast, compared to the Shannon capacity, **Fig. 6** shows that there are nearly identical gaps when $R=3$ and $R=5$ for β =2, meaning that the smaller R

is enough to achieve better performance when β is low. Otherwise, the larger R is necessary. Similar phenomena are observed in [24] as well.

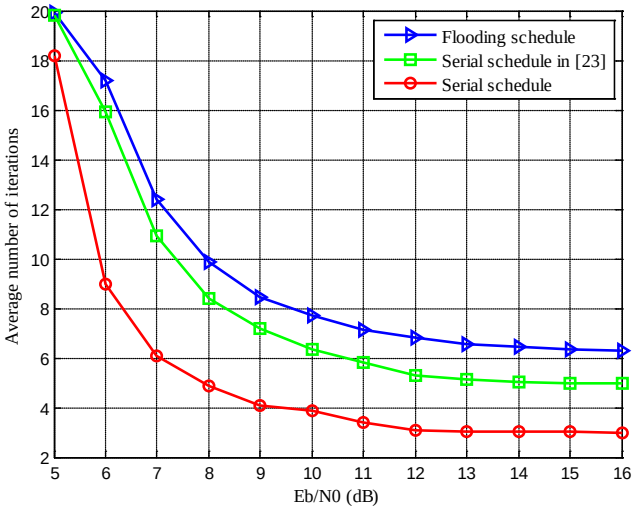

Fig. 7. Average number of iterations at different signal-to-noise ratios for different schedules, in which I = 20.

6.3 Convergence Speed

To gain insight into the convergence speed for different message schedule schemes of the JSG–SCDT, the average number of iterations required to correctly detect a symbol (i.e., the result of syndrome computing equals 0) at different SNRs is provided in **Fig. 7** when the maximum number of iterations is 20. As shown in the figure, when Eb/N0 = 13 dB, the symbols have been detected correctly after an average 6.6, 5.1, and 3.1 iterations due to syndrome computing for the flooding schedule, serial schedule in [23], and serial schedule, respectively, even though the interference among datastreams has not been canceled completely, as discussed in subsection 6.1. The average number of iterations required is nearly identical for the three schedules at Eb/N0 = 5 dB given the greater noise variance. The iterations required to correctly detect symbols keep nearly constant when Eb/N0 > 13 dB, since noise variance $\sigma_z^2 \to 0$ as SNR increases. Compared to the flooding schedule, at most 22% of iterations can be reduced by using the serial schedule proposed in [23]. Thus, the convergence speed accelerated is rather limited by using the algorithm proposed in [23] for JSG–SCDT. However, roughly more than half of the iterations can be spared by exploring the proposed serial schedule when Eb/N0 > 6 dB.

6.4 Performance Comparison

Fig. 8 shows the bit error rate (BER) and block error rate (BLER) results for different schemes with modulation loads of about 200% over the AWGN channel. Each datastream is modulated by using quadrature phase-shift keying. The BER and BLER curves of the JSG–CONV are given to clearly show the improved performance due to spatial coupling. As the figure shows, JSG–SCDT achieves the best performance by exploiting the advantages of both JSG and spatial coupling. The JSG–SCDT brings about 1- and 5-dB improvements in performance, with BER close to 10^{-5} over the JSG–CONV and SDD–SCDT, respectively. By comparison, the BER and BLER curves of turbo-structured joint demodulation and decoding based on JSG

for SCDT are plotted in **Fig. 8**. Turbo-structured joint demodulation and decoding involves the exchange of information between the detector and the decoder in a turbo manner, as applied in [25]. Five outer–inner turbo iterations are set between the detector and decoder, and 10 demodulation iterations and 10 decoding iterations are performed, while the maximization number of iterations of JSG–SCDT is set to 20. The symbol can be detected correctly at Eb/N0 = 7 dB when $I = 20$, as shown in the previous subsection. As the figure illustrates, although the complexity of JSG–SCDT is less than that of turbo-structured joint demodulation and decoding, the BER and BLER of JSG–SCD still outperform that of the turbo-structured receiver. Therefore, the JSG–SCDT can be regarded as an effective multiple access scheme to improve spectrum efficiency.

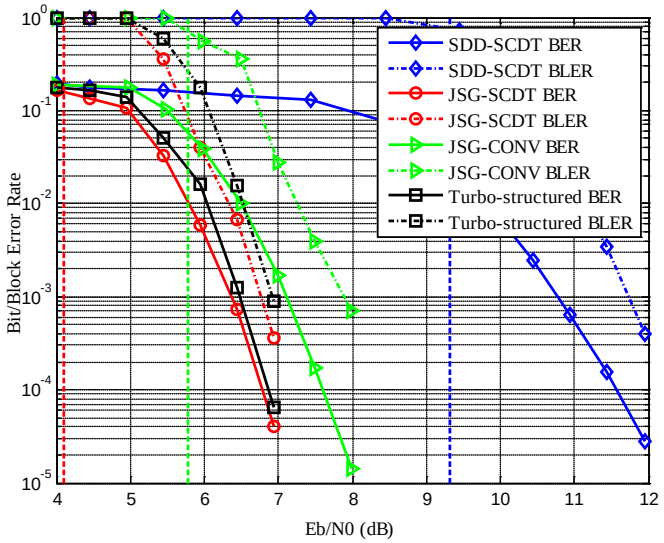

Fig. 8. Bit error rate (BER) and block error rate (BLER) versus Eb/N0 in dB for the joint sparse graph (JSG) for spatially coupling data transmission (SCDT), JSG for conventional structure (CONV), and separated demodulation and decoding (SDD) for SCDT, in which $L = 36$ and $\beta = 2$; vertical dashed lines show the decoding thresholds for the three schemes, as shown in Table 1.

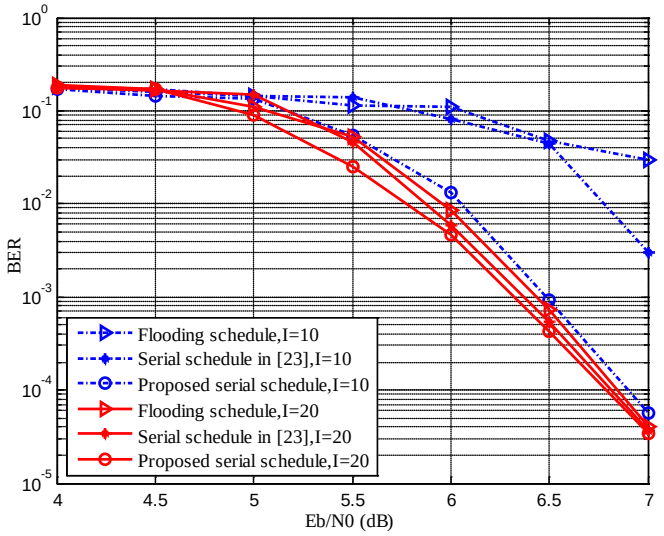

Fig. 9. Comparison of the performance of different message schedule schemes.

To show the system performance of the three different message schedule schemes of JSG–SCDT, their BER are given in **Fig.9** for brevity's sake. Clearly, the proposed serial schedule always achieves the best performance under the same number of iteration, since fresh updated messages of channel and check nodes join the iterative process immediately, whereas those messages can be used only in the next iteration in the flooding schedule. For the serial schedule proposed in [23], only the fresh information of the channel node can be applied in the current iteration. Consequently, it is possible to obtain more reliable information and accelerate the convergence speed for the proposed serial schedule than for other schedules. As shown in the figure, when I = 10, the performance of the proposed serial schedule is improved significantly over that of the others. However, the performances of the three schedule schemes are almost the same at Eb/N0 = 7 dB when I = 20. This phenomenon indicates that the schedules converge at the same point, as observed in [23]. Also, the performance of the proposed serial schedule at I = 10 is nearly the same as that of the flooding schedule at I = 20. Therefore, roughly half of the iterations can be reduced to attain the nearly same performance.

7. Conclusion

In this paper, a JSG–SCDT scheme has been proposed in order to enhance the spectrum efficiency and performance of iterative demodulation and decoding. Based on the JSG, the approach for iterative joint demodulation and decoding by BP has been presented by exploring the flooding schedule. The performance of the iterative joint demodulation and decoding of the JSG–SCDT and the iterative demodulation of the SDD–SCDT based on BP has been analyzed by DE in the large sparse system limit. Furthermore, the corresponding coupled equations about DE have been derived. Theory analysis and simulation results verify that the JSG–SCDT has a better convergence speed and higher decoding threshold than the SDD–SCDT and turbo-structured receiver. To further accelerate convergence speed and reduce the complexity of joint demodulation and decoding, a novel serial schedule has been proposed. Numerical results show that JSG–SCDT can yield an improvement in performance by about 5 dB over SDD–SCDT in a finite-sized system, and about half of the iterations can be spared under similar system performance conditions by using the proposed serial schedule, which can save half of the demodulation and decoding complexity.

Appendix

Assuming BPSK modulation, evaluating the evolution of marginal posterior probability is equivalent to tracing the evolution of the PDF of the LLR for the BP receiver [11]. For the BP demodulation of JSG–SCDT, the exact BP is applied to trace the evolution of the PDF of the channel node's LLR, whereas the GA is used to trace the evolution of the PDF of the check node's LLR for decoding JSG–SCDT.

We consider that the scalar Gaussian channel $Z = X + N$, in which Z, X, N are random variables and $N \sim \mathcal{N}\left(0, \gamma^{-1}\right)$, $X \in \{-1, +1\}$, and γ denotes the SNR. Let the LLRs $\left\{ L\left(Z \middle| x\right) = \ln \frac{p(Z|x=1)}{p(Z|x=-1)} \right\}_{x \in \mathbb{X}}$ be a random vector of a dimension equal to the cardinality of $\mathbb{X}$. For any channel $X \to Z$, if the LLR vector is Gaussian distributed, then its mean and variance can be expressed by

$$\begin{cases} E\left[L\left(Z|x\right)\right]=2\gamma x, \\ V\left[L\left(Z|x\right)\right]=4\gamma. \end{cases} \tag{21}$$

The channel must be statistically equivalent to the scalar Gaussian channel $Z=X+N$ [20]. Therefore, we give two steps to prove Theorem 1.

First, we prove that the LLR (8) vector is Gaussian distributed. For regular LDPC codes, the output LLR $L^{(i)}_{c_{\tilde{j},\tilde{l}}\to v_{m,l}}$ of a check node is Gaussian, and the output LLRs of all the check nodes are independent and identically distributed [22]. Therefore, $\sum_{(\tilde{j},\tilde{l})\in\varphi(m,l)} L^{(i)}_{c_{\tilde{j},\tilde{l}}\to v_{m,l}}$ is Gaussian because the sum of independent Gaussian random variables is also Gaussian. The ACF property of **H** guarantees that incoming LLRs from the channel are independent random variables in the large system limit. Thus, $\sum_{(\tilde{n},\tilde{t})\in\beta(m,l)} L^{(i)}_{s_{\tilde{n},\tilde{t}}\to v_{m,l}}$ converges in law to a Gaussian distribution using the central limit theorem. Therefore, the LLR (8) is Gaussian distributed because the sum of two Gaussian distributions that are independent is Gaussian as well.

Second, we prove that the mean and variance of the LLR of the variable node could be expressed by using (21). As proven in [11], the equivalent channel for BP demodulation with GA converges to the asymptotic equivalent channel for true BP demodulation. Therefore, we derive the mean and variance of the channel node LLR by using the exact BP demodulation following [11] and [20] and prove that the mean and variance of the channel node LLR converge to

$$\begin{cases} \mathrm{E}[\sum_{(\tilde{n},\tilde{t})\in\beta(m,l)} L^{(i)}_{s_{\tilde{n},\tilde{t}}\to v_{m,l}}]\to 2s\tilde{i}r^{(i)}_{l}b_{m,l}, \\ V[\sum_{(\tilde{n},\tilde{t})\in\beta(m,l)} L^{(i)}_{s_{\tilde{n},\tilde{t}}\to v_{m,l}}]\to 4s\tilde{i}r^{(i)}_{l} \end{cases} \tag{22}$$

in the large sparse system limit, in which

$$s\tilde{i}r^{(i)}_{l}=\frac{1}{K}\sum_{r=0}^{R-1}\frac{1}{\sigma^2_{(r+\lfloor l/\beta\rfloor)}(i)}, \tag{23}$$

with

$$\sigma^2_t(i)=\sigma^2_z+\frac{1}{K}\sum_{k=0}^{K_t-1}\zeta^{(i-1)}_{[k+(t-R+1)\beta]}, \tag{24}$$

and $(t-R+1)\beta=0$ when $t\le 1$, K_t denotes the number of superposition datastreams at one instant during time t, and $K_t\in[\beta,K]$ for all $t\in\mathcal{T}$. The $\zeta^{(i)}_l$ are denoted by

$$\zeta^{(i)}_l=\mathrm{E}[(b_{\tilde{m},\tilde{l}}-\mathrm{E}(b^{(i)}_{\tilde{m},\tilde{l}}))^2], \tag{25}$$

in which $\mathrm{E}[b^{(i)}_{m,l}]$ denotes the posterior mean estimator of $b_{m,l}$ in iteration i.

The LLR of check node of regular LDPC codes is calculated by GA [22] and given by

$$\rho^{(i)}_u=\Phi^{-1}\left(1-[1-\Phi(\rho_{u_0}+(d_v-1)\rho^{(i-1)}_u)]^{d_c-1}\right), \tag{26}$$

in which the function $\Phi(\cdot)$ is defined in [22], and ρ_{u_0} denotes the mean of LLR u_0, which is from the channel. Since the LLR from the channel is $\sum_{(\tilde{n},\tilde{t})\in\beta(m,l)} L^{(i)}_{s_{\tilde{n},\tilde{t}}\to v_{m,l}}$ for the JSG–SCDT and variable in each iteration. With a slight abuse of notation, ρ_{u_0} is denoted by $\rho^{(i)}_{u_0}$ and

$\rho_{u_0}^{(i)} = 2\tilde{sir}_l^{(i)} b_{m,l}$, then (14) is obtained, and the mean and variance of the second term $\sum_{(\tilde{j},\tilde{l})\in\varphi(m,l)} L_{c_{\tilde{j},\tilde{l}}\to v_{m,l}}^{(i)}$ of (8) are given by

$$\begin{cases} \mathrm{E}[\sum_{(\tilde{j},\tilde{l})\in\varphi(m,l)} L_{c_{\tilde{j},\tilde{l}}\to v_{m,l}}^{(i)}] = d_v \rho_u^{(i)} b_{m,l}, \\ V[\sum_{(\tilde{j},\tilde{l})\in\varphi(m,l)} L_{c_{\tilde{j},\tilde{l}}\to v_{m,l}}^{(i)}] = 2d_v \rho_u^{(i)} \end{cases} \tag{27}$$

in the large sparse system limit. Consequently, the mean and variance of LLR (8) converge to

$$\begin{cases} \mathrm{E}[L_{v_{m,l}}^{(i)}] = \mathrm{E}[\sum_{(\tilde{n},\tilde{t})\in\beta(m,l)} L_{s_{\tilde{n},\tilde{t}}\to v_{m,l}}^{(i)}] + \mathrm{E}[\sum_{(\tilde{j},\tilde{l})\in\varphi(m,l)} L_{c_{\tilde{j},\tilde{l}}\to v_{m,l}}^{(i)}] \to 2sir_l^{(i)} b_{m,l}, \\ V[L_{v_{m,l}}^{(i)}] = V[\sum_{(\tilde{n},\tilde{t})\in\beta(m,l)} L_{s_{\tilde{n},\tilde{t}}\to v_{m,l}}^{(i)}] + V[\sum_{(\tilde{j},\tilde{l})\in\varphi(m,l)} L_{c_{\tilde{j},\tilde{l}}\to v_{m,l}}^{(i)}] \to 4sir_l^{(i)} \end{cases} \tag{28}$$

with

$$sir_l^{(i)} = \tilde{sir}_l^{(i)} + \frac{d_v}{2}\rho_u^{(i)}. \tag{29}$$

Thus, the mean and variance (28) of the variable node LLR can be expressed by using (21), respectively.

References

[1] IMT-2020(5G) Promotion Group, 5G Vision and Requirements. May, 2014. Article (CrossRef Link)

[2] Tao Y, Liu L, Liu S, et al, "A survey: Several technologies of non-orthogonal transmission for 5G," *China Communications*, vol. 12, no. 10, pp. 1-15, 2015. Article (CrossRef Link)

[3] Dai L, Wang B, Yuan Y, et al., "Non-orthogonal multiple access for 5G: Solutions, challenges, opportunities, and future research trends," *IEEE Communications Magazine*, vol. 53, no. 9, pp. 74-81, 2015. Article (CrossRef Link)

[4] Felström A J, Zigangirov K S., "Time-varying periodic convolutional codes with low-density parity-check matrix," *IEEE Transactions on Information Theory*, vol. 45, no. 6, pp. 2181-2191, 1999. Article (CrossRef Link)

[5] Kudekar S, Richardson T J, Urbanke R L,"Threshold saturation via spatial coupling: Why convolutional LDPC ensembles perform so well over the BEC," *IEEE Transactions on Information Theory*, vol. 57, no. 2, pp. 803-834, 2011. Article (CrossRef Link)

[6] Kudekar S, Richardson T, Urbanke R L, "Spatially coupled ensembles universally achieve capacity under belief propagation," *IEEE Transactions on Information Theory*, vol. 59, no. 12, pp. 7761-7813, 2013. Article (CrossRef Link)

[7] Truhachev D, Schlegel C, "Spatially coupled streaming modulation," in *Proc. of IEEE International Conference on Communications*, pp. 3418-3422, June 9-13, 2013. Article (CrossRef Link)

[8] Truhachev D, "Achieving AWGN multiple access channel capacity with spatial graph coupling," *IEEE Communication Letters*, vol. 16, no. 5, pp. 585-588, 2012. Article (CrossRef Link)

[9] Schlegel C and Truhachev D, "Multiple access demodulation in the lifted signal graph with spatial coupling," *IEEE Transactions on Information Theory*, vol. 59, no. 4, pp. 2459-2470, 2013. Article (CrossRef Link)

[10] Takeuchi K, Tanaka T, Kawabata T, "Improvement of BP-based CDMA multiuser detection by spatial coupling," in *Proc. of IEEE International Symposium on Information Theory*,pp.1489-1493, July 31-Aug. 5 , 2011. Article (CrossRef Link)

[11] Takeuchi K, Tanaka T, Kawabata T, "Performance improvement of iterative multiuser detection for large sparsely spread CDMA systems by spatial coupling," *IEEE Transactions on Information Theory*, vol. 61, no. 4, pp. 1768-1794, 2015. Article (CrossRef Link)
[12] Kudekar S, Pfister H D, "The effect of spatial coupling on compressive sensing," in *Proc. of the 48th IEEE Communication, Control, and Computing* , pp. 347-353, 2010. Article (CrossRef Link)
[13] Donoho D L, Maleki A, Montanari A, "Message-passing algorithms for compressed sensing," in *Proc. of the National Academy of Sciences*, vol. 106, no. 45, pp. 18914-18919, 2009. Article (CrossRef Link)
[14] Yedla A, Pfister H D, Narayanan K R, "Universality for the noisy Slepian-Wolf problem via spatial coupling," in *Proc. of IEEE International Symposium on Information Theory*, pp.2567-2571, 2011. Article (CrossRef Link)
[15] Hassani S H, Macris N, and Urbanke R L. (Dec. 2011), "Threshold saturation in spatially coupled constraint satisfaction problems" [Online]. Available: http://arxiv.org/abs/1112.6320. Article (CrossRef Link)
[16] Liu Z, Guo, Y, et al., "Fast convergence of joint demodulation and decoding based on joint sparse graph for spatially coupling data transmission," in *Proc. of* the *27th Annual International Symposium on Personal, Indoor, and Mobile Radio Communication (PIMRC)*, Sept 4-8, 2016. Article (CrossRef Link)
[17] Wen L, Razavi R, Imran M A, et al, "Design of joint sparse graph for OFDM system," *IEEE Transactions on Wireless Communications*, vol. 14, no. 4, pp. 1823-1836, 2015. Article (CrossRef Link)
[18] Lentmaier M, Sridharan A, Zigangirov K S, et al, "Terminated LDPC convolutional codes with thresholds close to capacity," in *Proc. of IEEE International Symposium on Information Theory*, pp.1372-1376, 2005. Article (CrossRef Link)
[19] Pearl J, "Probabilistic reasoning in intelligent systems: Networks of plausible inference," Morgan Kaufmann, 2014. Article (CrossRef Link)
[20] Guo D, Wang C C, "Multiuser detection of sparsely spread CDMA," *IEEE Journal on Selected Areas in Communications*, Vol 26, no 3, pp.421-431, 2008. Article (CrossRef Link)
[21] Richardson T J, Urbanke R L, "The capacity of low-density parity-check codes under message-passing decoding," *IEEE Transactions on Information Theory*, vol. 47, no. 2, pp. 599-618, 2001. Article (CrossRef Link)
[22] Chung S Y, Richardson T J, Urbanke R L, "Analysis of sum-product decoding of low-density parity-check codes using a Gaussian approximation," *IEEE Transactions on Information Theory*, vol. 47, no. 2, pp. 657-670, 2001. Article (CrossRef Link)
[23] Wen L, Razavi R, Xiao P, et al., "Fast convergence and reduced complexity receiver design for LDS-OFDM system," in *Proc. of the 25th Annual International Symposium on Personal, Indoor, and Mobile Radio Communication (PIMRC)*, pp.918-922, September 2-5, 2014. Article (CrossRef Link)
[24] Song G, Cheng J, Watanabe Y, "Maximum sum rate of repeat-accumulate interleave-division system by fixed-point analysis," *IEEE Transactions on Communications*, vol. 60, no. 10, pp. 3011-3022, 2012. Article (CrossRef Link)
[25] Razavi M, Al-Imari M, Imran A, Hoshyar R, and Chen D, "On receiver design for uplink low density signature OFDM (LDS-OFDM)," *IEEE Transactions on Communications*, vol. 60, no. 11, pp. 3499-3508, 2012. Article (CrossRef Link)

Zhengxuan Liu is currently a Ph.D. candidate at Beijing University of Posts and Telecommunications, Beijing, China. After working in the Institute of Optoelectronic Technology East China, Anhui Province for a year, he worked at ZTE Corporation as a software engineer from 2010 to 2013. His research interests include multiple access and channel coding.

Guixia Kang is a professor and PhD tutor at Beijing University of Posts and Telecommunications (BUPT). She currently as the group leader of the Ubiquitous Healthcare Working Group of China's Ubiquitous Network Technologies and Development Forum, executive vice director of E-health Professional Commission of China Apparatus and Instrument Association, one of four domestic Smart Medicine Specialists of China Smart City Forum, and a member of ITU-R 8F - China Working Group, etc. Her research interests include wireless transmission technologies in PHY and MAC layers. Besides, she is also the founder of wireless eHealth (WeHealth)and works on its technology, standardization and application.

Zhongwei Si received her Ph.D. degree in telecommunications from KTH-Royal Institute of Technology (Sweden) in January 2013. In August 2013, she joined Beijing University of Posts and Telecommunications, where she currently serves as a lecturer. Dr. Si has been dedicated to PHY layer techniques in wireless communications for years. Her research interests include future wireless communication, information theory, advanced channel coding, etc.

Ningbo Zhang received the Ph.D. degrees at Beijing University of Posts and Telecommunications (BUPT) in 2010. He worked in Huawei Technology from 2010 to 2014. He currently is a lecture of BUPT. His major research interests include wireless communication theory, machine to machine communications, multiple access, cognitive radio and signal processing.